**UNIVERSITEIT
AMSTERDAM**

VU Research Portal

Mechanisms of H2 dissociative adsorption on the Pt(211) stepped surface

McCormack, D.A.; Olsen, R.A.; Baerends, E.J.

document version
Publisher's PDF, also known as Version of record

Link to publication in VU Research Portal

citation for published version (APA)
McCormack, D. A., Olsen, R. A., & Baerends, E. J. (2005). Mechanisms of H2 dissociative adsorption on the Pt(211) stepped surface. *Journal of Chemical Physics*, *122*(19), 194708. https://doi.org/10.1063/1.1900087

Mechanisms of H₂ dissociative adsorption on the Pt(211) stepped surface

Drew A. McCormack[a)]
*Theoretische Chemie, Faculteit Exacte Wetenschappen, Vrije Universiteit, De Boelelaan 1083,
1081 HV Amsterdam, The Netherlands*

Roar A. Olsen
*Leiden Institute of Chemistry, Gorlaeus Laboratories, Leiden University, P.O. Box 9502, 2300 RA Leiden,
The Netherlands*

Evert Jan Baerends
*Theoretische Chemie, Faculteit Exacte Wetenschappen, Vrije Universiteit, De Boelelaan 1083,
1081 HV Amsterdam, The Netherlands*

We utilize classical trajectory calculations to study the reaction dynamics of the dissociative adsorption of H₂ on the stepped Pt(211) surface. The potential-energy surface has been obtained through an accurate interpolation of density-functional theory data at the generalized gradient approximation level, using the corrugation reduction procedure. New techniques for visualizing the collective dynamics of trajectories are introduced to elucidate the reaction mechanisms involved. Reaction exhibits a nonmonotonic dependence on collision energy, first decreasing with energy, and then increasing. A strong component of direct nonactivated reaction exists at the top edge of the step over the entire range of energies. The inverse relationship between reaction and collision energy at low energies is attributed to trapping in weak chemisorption wells. These wells also influence the direct reaction at the step, leading to a strong asymmetric dependence on incidence angle. Reaction on the terrace is activated, and only contributes significantly at high energies. Agreement with experiments on Pt(533) [A. T. Gee, B. E. Hayden, C. Mormiche, and T. S. Nunney, J. Chem. Phys. **112**, 7660 (2000); Surf. Sci. **512**, 165 (2002)] is good, and we are able to suggest new interpretations of the experimental data. © *2005 American Institute of Physics*.
[DOI: 10.1063/1.1900087]

I. INTRODUCTION

The role of steps in gas-surface reactions is still largely a mystery, despite empirical evidence that their presence enhances reactivity.[1] Until recently, not even the site of reaction could be rigorously established, let alone the reactive mechanisms involved. Some authors advocated that the steps themselves dominated reaction,[2] while others espoused that reaction at other sites was equally important.[3]

A recent series of experimental studies by Hayden and co-workers have been very enlightening as regards the reaction sites and mechanisms of stepped-surface systems.[4–6] Experiments on hydrogen reaction occurring on the Pt(533) surface—a close relative of the title reaction in this study—revealed that reaction occurred on both the steps and terraces.[5,6] They identified two direct high-energy mechanisms, the dominant one being ascribed to the (111) terrace and the weaker to the step, and two low-energy indirect mechanisms. The first indirect mechanism, active only below 30 meV, was temperature dependent, and was attributed to an accommodated physisorption precursor. The second, active up to 150 meV, was temperature independent, and thought to result from an unaccommodated precursor with subsequent reaction at the step.

Theoretical methods have advanced to the point that dissociative adsorption can be accurately modeled,[7] largely thanks to the improved evaluation of molecule-surface interaction made possible by density-functional theory[8] (DFT) at the generalized gradient approximation (GGA) level;[9] however, few theoretical studies have been directed at reaction dynamics on stepped surfaces. The unit cell of a stepped surface tends to be much larger than for a flat single-crystal surface, and this makes manufacturing a potential-energy surface (PES) to describe the gas-surface interaction considerably more expensive. Even with a PES in hand, quantum dynamics calculations for stepped systems are difficult, requiring larger basis sets to account for the increased density of diffraction states and low symmetry.

Though stepped surfaces have not come under the close scrutiny of the theoreticians, flat surfaces have, and much can be learned from this body of work. Stepped-surface reactions tend to be nonactivated, making nonactivated flat-surface reactions most relevant. The reaction probability of such systems exhibit an intriguing dependence on the collision energy of the gas molecules, first decaying with increasing energy, and then rising at higher energies. The low-energy behavior is quite counterintuitive—reactivity can be *increased* by *decreasing* the energy of the reactant gas molecule.

This type of behavior has traditionally been ascribed to molecular trapping in a physisorption precursor state, but in

---

[a)]Electronic mail: da.mccormack@few.vu.nl

122, 194708-1

the 1990s a new explanation was presented: *dynamical steering*.[10,11] Dynamical steering is a direct reaction mechanism in which molecules approaching the surface can be gradually steered into the most favorable geometry for reaction. Slower moving molecules have more time to undergo steering, adiabatically following the minimum-energy path, thus leading to increased reactivity with decreasing energy.

Steering has since become a fashionable explanation for the nonmonotonic energy dependence of reaction, but more recent works by Busnengo and co-workers have moved thinking back in favor of precursorlike mechanisms.[12–19] Classical trajectory calculations on high-quality DFT PESs for Pd(111) (Ref. 20) and Pd(110) (Ref. 17) have shown that the upturn in reaction at low energies is due to *dynamical trapping*. Dynamical trapping occurs when energy redistribution amongst the internal degrees of freedom of an incident molecule leaves it with too little energy in the motion away from the surface to escape. Dynamical trapping can occur if the PES has a well, but can also arise in the absence of a "real" well: excitation of internal degrees of freedom may lead to a well in the "dynamical PES" governing the molecule's motion. An example of this are the resonant states that arise when hydrogen reacts on Cu(100);[21,22] these are due to a weakening of the dimer bond as the molecule approaches the surface, leading to a well in the adiabatic potentials of vibrationally excited states.[22]

Busnengo *et al.* have looked at numerous aspects of hydrogen reaction on flat palladium surfaces. They found that trapping essentially involved translational-to-rotational (T →R) energy transfer, and that aspects of the PES in the entrance channel could profoundly influence the dynamics.[13,15] They showed that energy exchange between surface phonons and trapped molecules could occur, and were able to explain experimental findings for inelastic rotational scattering.[14] More recently, they used classical and quantum techniques to study the effect of rotational excitation on reaction, finding that trapping was quenched by the rotational motion.[18,19] A further study of off-normal scattering showed that translational motion normal to the surface was efficiently converted into rotational motion of the back-scattered molecules.[16]

We recently presented the first six-dimensional (6D) PES for a diatomic molecule (H_2) interacting with a stepped surface [Pt(211)].[23] This PES was obtained through an accurate interpolation of DFT/GGA data using the corrugation reduction procedure,[20,24] and was used in classical calculations of the reaction dynamics. We were able to reproduce the nonmonotonic dependence of reaction for normal incidence, and showed nonactivated sites atop step atoms dominated the reaction. Direct reaction occurred above the steps at all energies, and at low energy an indirect mechanism was also active: molecules could become dynamically trapped in a weak chemisorption well located at the join between the bottom edge of the step and the terrace. These molecules had an increased probability of migrating to the reactive step and dissociating.

In this study we extend our previous work with a more thorough breakdown of the reaction mechanisms involved, including high-energy reaction on the terrace. We also con-

sider off-normal incidence, and make detailed comparisons with the results of Hayden and co-workers for hydrogen reaction on Pt(533).[5,6] The classical dynamics capably reproduces the experimental results, and provides great insight into the mechanisms from which they arise. New visualization techniques are developed to aid this analysis of the classical dynamics.

In Sec. II we detail how the PES was constructed, and the method used to calculate the reaction dynamics. Section III presents results and discussion, covering reaction at off-normal incidence, site dependence of reaction, directness of reaction, and angular dependence of the scattered molecules. Results are compared with the experimental work of Hayden and co-workers,[5,6] and the experimental results interpreted in light of the classical trajectory study. Conclusions are drawn in Sec. IV, and the Appendix A describes the techniques used for visualizing collective classical dynamics.

II. METHOD

A. Construction of a 6D PES for H_2+Pt(211)

The program ADF-BAND (Ref. 25) was used to solve the Kohn–Sham equations[8] self-consistently within a linear combination of atomic orbitals approach, for a H_2 molecule adsorbed on a Pt(211) surface, modeling the surface by a slab with translational symmetry in two directions. A GGA combining the Becke correction[26] for the exchange energy with the Perdew correction[27] for the correlation energy was employed. All aspects of these periodic DFT/GGA calculations have been discussed in detail in Refs. 28 and 29.

To interpolate the DFT/GGA data we have chosen to employ the corrugation reduction procedure.[20] This method has been proven to provide very accurate interpolation results for H_2 molecules interacting with several metal surfaces.[17,20,24,30] The crux of the method is that the interpolation is not carried out on the rather corrugated DFT/GGA data itself (V^{6D}), but on the much smoother interpolation function (I^{6D}) obtained by subtracting the separate interactions of each atom of the hydrogen molecule with the surface ($R_{H(1)}^{3D}$ and $R_{H(2)}^{3D}$):

$$I^{6D} = V^{6D} - R_{H(1)}^{3D} - R_{H(2)}^{3D}. \tag{1}$$

Because the PES describing the interaction of atomic hydrogen with the surface (R_H^{3D}) is rather corrugated itself, the technique is applied a second time. The atomic interpolation function (I^{3D}) is interpolated, rather than the atomic potential itself:

$$I^{3D} = R_H^{3D} - \sum_{i=0}^{n} Q^{1D}(r_i), \tag{2}$$

where Q^{1D} is the interaction potential between a single Pt atom and a single H atom, and the sum runs over all Pt atoms in the slab (r_i is the distance between the H atom and the ith Pt atom). The "pair-potential" Q^{1D} is obtained from a spline interpolation of about 40 DFT/GGA data points. The interpolation of the atomic PES is based on about 850 DFT/GGA data points above 24 sites on the surface, using spline interpolation along Z, and symmetry-adapted basis functions
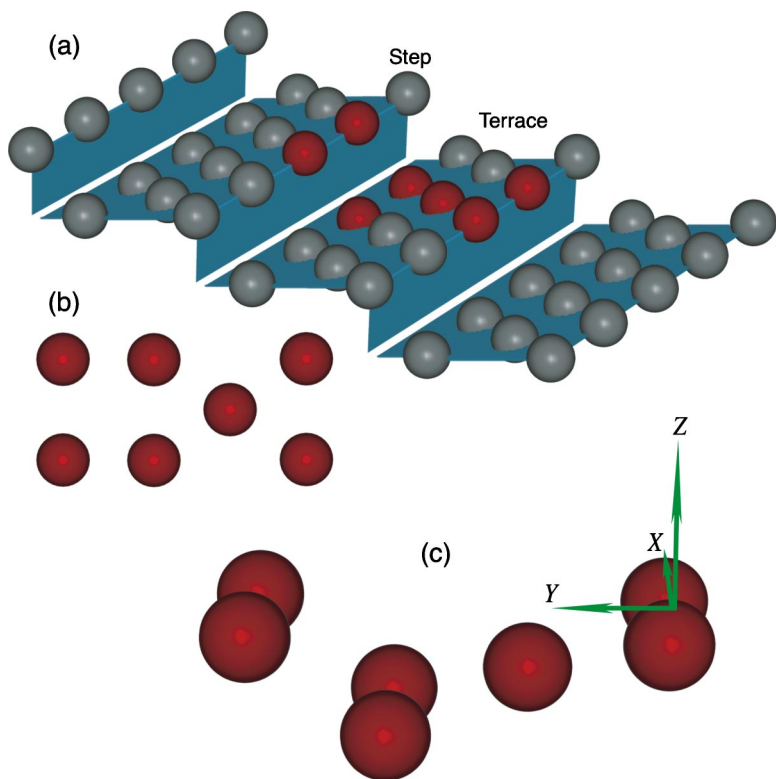
FIG. 1. (Color) The Pt(211) surface and coordinate system. (a) The surface atoms and stepped structure of Pt(211), with one unit cell highlighted. The step and terrace sites are labeled. (b) The surface atoms in the unit cell of Pt(211) shown from above. (c) The coordinate system shown with respect to a side view of the Pt(211) unit cell. X, Y, and Z are the Cartesian coordinates of the center of mass of a hydrogen molecule, with the origin positioned on a top-of-step surface atom. X points along the top of the step from one atom to the next, Y points perpendicular to the step, from one step atom to the next, and Z is normal to the surface. The internal coordinates of hydrogen (not shown) are the bond length r, the polar angle taken with respect to the positive Z axis θ, and the azimuthal angle taken with respect to the positive X axis ϕ.

along X and Y (see Ref. 24 for a general description of this approach). The 24 surface sites stem from three sets of eight equidistantly spaced surface sites along the lines $X=0$, $X=1.31a_0$, and $X=2.62a_0$, respectively (see Ref. 28 for more detail). The molecular PES is based on more than 100 two-dimensional (Z,r) cuts above the same 24 surface sites, including enough molecular orientations at each surface site to describe the symmetry correctly. About 10 000 DFT/GGA data points have been used in the interpolation of the molecular PES, with splines used for (Z,r) and symmetry-adapted basis functions for (X,Y,θ,ϕ) (Ref. 24). The resulting root-mean-square (maximal) error is around 20 (50) meV, when tested against 350 DFT/GGA data points *not* included in building the PES.

B. Classical trajectory calculations

Classical dynamics calculations were performed with 10 000 trajectories propagated for each initial state (unless stated otherwise). Microcanonical sampling was used, resulting in the same total energy for each trajectory of a given initial state. Each trajectory in an ensemble was imparted the same translational energy and velocity relative to the surface. Trajectories were initiated with no vibrational energy. Each molecule was randomly oriented, with no rotational motion (corresponding to rotational state $j=0$).

Propagation of trajectories was performed in Cartesian coordinates with the 4th-order Runge–Kutta algorithm[31] and a fixed time step of 5 a.u. Trajectories were initiated at $Z=6.5a_0$, where Z is the distance from the surface to the H$_2$ center of mass (Fig. 1). Reaction of a trajectory was deemed to have occurred when the H–H bond length (r) exceeded

4.5a_0. Any trajectory for which $Z>6.6a_0$ was considered backscattered.

Some care needs to be taken in the choice of phase space sampled to generate microcanonical initial conditions. Two common approaches exist: *classical* and *quasiclassical*. In the former instance, no vibrational energy is imparted on the molecules, corresponding to the classical zero point. Quasiclassical calculations impart energy equal to the quantum zero-point value on each molecule. It is now well known that these two approaches perform better under different circumstances. The quasiclassical method works best for activated systems,[32] but suffers from the so-called zero-point energy problem[33] when long-lived trajectories arise. Basically, the ZPE that would quantally be conserved as vibrational motion is classically able to flow into other modes, opening up pathways that would otherwise be energetically inaccessible. When used with a system that should exhibit molecular trapping, for example, quasiclassical trajectory calculations typically do not get trapped, because the vibrational ZPE can be used to escape the trapping well.[15,17]

Classical trajectory calculations are known to greatly underestimate reaction for activated systems, because there is no vibrational energy available to assist barrier crossing;[32] however, for nonactivated systems, classical trajectories work quite well,[15,34] avoiding problems that arise due to energy leaking out of the vibrational modes. It is possible to improve on classical mechanics somewhat by effectively modifying the PES to account for adiabatic changes in vibrational ZPE as a molecule approaches the surface.[15] Here we have opted to use the unadulterated PES: results should be qualitatively correct and quantitatively reasonable even without accounting for changes in the vibrational frequency.

III. RESULTS AND DISCUSSION

A. Details of the PES

Figure 2 shows several contour plots of the H_2 +Pt(211) PES that we have constructed. Figures 2(a)–2(d) are for various two-dimensional (2D) cuts through the PES, at strategically chosen locations in the unit cell. Figure 2(c), which is directly above the central atom of the terrace, exhibits an early barrier to reaction. Figure 2(d) shows that atop the step atoms, there is no barrier to reaction. Figures 2(a) and 2(b) and are for nonreactive sites (at the energies of interest here, i.e., <0.30 eV), but they show the presence of shallow chemisorption wells in the PES.

Figure 2(e), which is a contour plot in a plane parallel to the surface, also shows these wells, which occur above the join between the terrace and the lower edge of the step. There is a small barrier between the two wells, and another barrier between the deeper well and the nonactivated step site. These wells are not artifacts of the cut taken through the PES, but are real wells in the 6D PES. The equilibrium geometry of the shallow (terrace-side) well has a potential value of −34 meV for optimum coordinates ($X=1.48a_0, Y=6.81a_0, Z=3.86a_0, r=1.43a_0, \theta=98.0°, \phi=107.2°$). This geometry corresponds to H_2 with its bond marginally extended from the gas phase equilibrium, and oriented with its axis pointing in the direction of the top-edge step atom. The deeper (step-side) well has an equilibrium potential of −124 meV and coordinates ($X=1.26a_0, Y=9.76a_0, Z=4.00a_0, r=1.45a_0, \theta=147.4°, \phi=81.3°$), which is a more vertical orientation.

Figures 2(f)–2(h) are for vertical planes running parallel to the Y axis. The shallow wells can be clearly seen in Fig. 2(g). Figures 2(f) and 2(h) show small regions that are below the gas phase minimum energy. (The very low energies at either end of the unit cell are due to the very attractive top-of-step atoms, and are not wells.) These correspond to transition states between the symmetrically equivalent shallow wells within a single unit cell [Fig. 2(f)], and shallow wells in neighboring unit cells [Fig. 2(h)]. These transition states make molecular diffusion possible even at very low energies, as will be demonstrated below.

B. Off-normal reaction probabilities

Figure 3 shows reaction probabilities for off-normal incidence. At low collision energies, all plots decline with increasing collision energy, and indicate an insensitivity to incidence angle. This is most explicit in Fig. 3(d), where the plot for the 5-meV collision energy is almost flat, obeying total-energy scaling.

At higher energies, reaction is more complex. With a component of motion in the −Y direction [Fig. 3(b)], reaction tends to decline with increasing angle of incidence, apart from at the highest energies (>0.15 eV), where plots for small incidence angles tend to cross and overlap. The results for motion parallel to the +Y axis are far more convoluted [Fig. 3(a)]: between about 20 and 100 meV, reaction increases with angle of incidence; above 100 meV, probabilities are similar for all angles of incidence.

Considering the angular dependence of reaction for a fixed collision energy [Fig. 3(d)] can help clarify the other plots. We have already observed that for 5 meV, reaction was relatively independent of incidence angle. For 50 meV, the apparently different dependencies found in Figs. 3(a) and 3(b) hide a simple linear trend [Fig. 3(d)], with reaction decreasing with incidence angle. Motion parallel to the +Y axis is more favorable for reaction than motion parallel to −Y.

Figure 3(d) shows that angular dependence of reaction at high collision energies (i.e., 0.25 eV) does not follow a simple trend. For motion parallel to the +Y axis, there is little dependence on angle, as observed above, and for motion in −Y, reaction drops off with increasing off-normal incidence. Interestingly, the curve has a peculiar kink at −30°, suggesting that it may be comprised of two independent components: for negative angles, the curve initially parallels the 50-meV plot, and for positive angles, it is reminiscent of a normal energy scaling dependence, with a peak at around 20°. This angle corresponds closely to the normal to the terrace, suggesting that the two components observed may result from reaction on two different surface sites, probably the step and the terrace. We will examine this further below.

Plots for reaction at off-normal incidence with a component of momentum parallel to the X axis are shown in Fig. 3(c). Reaction tends to decrease with angle at most collision energies. It should be noted that reaction does not scale with normal energy, even at the highest collision energy shown. This is simple to check by comparing the plot for 0° with that for 60°. Normal energy scaling would dictate that the reaction probability for 60° should be $\cos^2(60°)=0.25$ times that for normal incidence, i.e., 0.135; the actual value for 60° is around twice as large. This same observation can also be made for reaction with motion in the Y direction—normal energy scaling is not observed in any of the results shown in Fig. 3.

C. Visualizations of reaction dynamics

Before moving on to more quantitative aspects of the reaction, we will now present a series of visualizations. The objective of performing these visualizations is to gain insight into the mechanisms involved, making the interpretation of results easier. The techniques used to generate the visualizations are explained in the Appendix A.

Figure 4 shows the time evolution of an isosurface of the density of H_2 bond center points for molecules incident normally at 5 meV. Two green-colored surfaces are visible in Fig. 4(a). These surfaces represent the projection of isosurfaces infinite in X and Y onto a single unit cell. The surfaces are for the same contour value, with the density of bond centers sandwiched between the sheets greater than that outside. All trajectories are initiated at the same time and distance from the surface, with an even distribution across the surface. This results in isosurfaces that are initially flat, and at a finite separation. The finite separation is purely an artifact of the fitting scheme used to form the continuous density from the discrete bond centers (see Appendix A). [The initial isosurfaces are not shown in Fig. 4(a).]

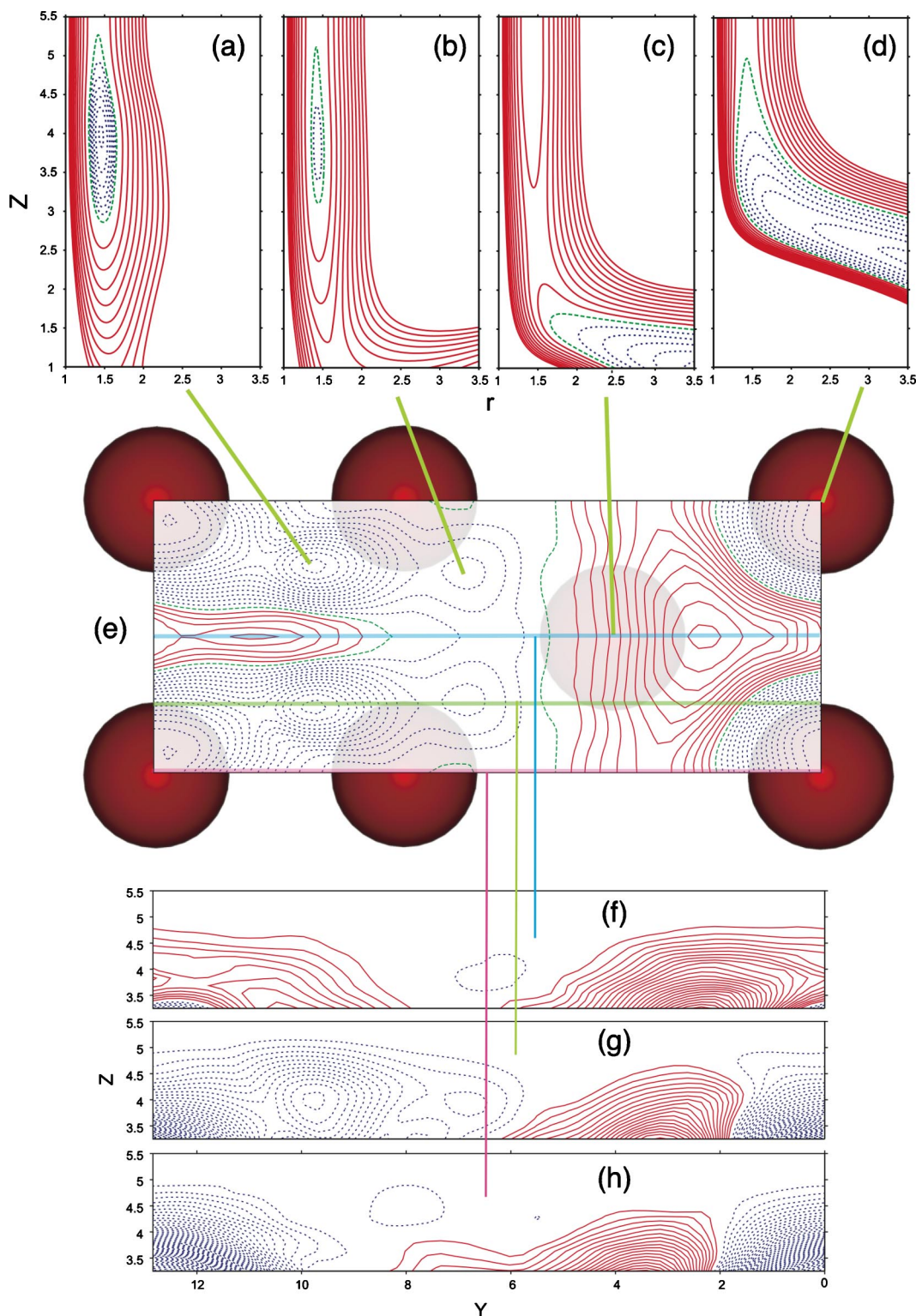Figure 4(a) shows the isosurface as it approaches the

FIG. 2. (Color) The H$_2$+Pt(211) potential-energy surface (PES). (a) A two-dimensional (2D) r-Z cut with the other coordinates corresponding to the equilibrium geometry of a well in the PES ($X=1.26a_0$, $Y=9.76a_0$, $\theta=147.4°$, $\phi=81.3°$). (b) A 2D r-Z cut with the other coordinates chosen to correspond with the equilibrium geometry of a shallower well ($X=1.48a_0$, $Y=6.81a_0$, $\theta=98.0°$, $\phi=107.2°$). (c) A 2D r-Z cut through the PES above the central terrace atom ($X=4.27a_0$, $Y=2.62a_0$, $\theta=90°$, $\phi=90°$). (d) A 2D r-Z cut for a molecule located above a top-of-step surface atom ($X=0$, $Y=0$, $\theta=90°$, $\phi=90°$). In (a)–(d), all positive contours are shown as solid red lines, at intervals of 100 meV. Negative contours are given as dotted blue lines. In (a) and (d), the negative contours are at intervals of 100 meV, while in (b) and (c) they are at intervals of 20 meV. The zero contour in (a)–(d) is shown as a dashed green line. (e) Contour plot for a plane parallel to the surface, at $Z=4.00a_0$. At each point in the plane, the remaining coordinates (r, θ, ϕ) are optimized to give the minimum potential. (f)–(h)Similarly optimized contour plots, but for vertical Y-Z planes at $X=2.62a_0$, $1.31a_0$ and $0.00a_0$, respectively. In (e)–(h), positive contours are shown as solid red lines, at intervals of 100 meV. Negative contours are dotted blue lines separated by 10 meV. A green dashed line in (e) represents the zero contour. The zero contour is not shown in (f)–(h).
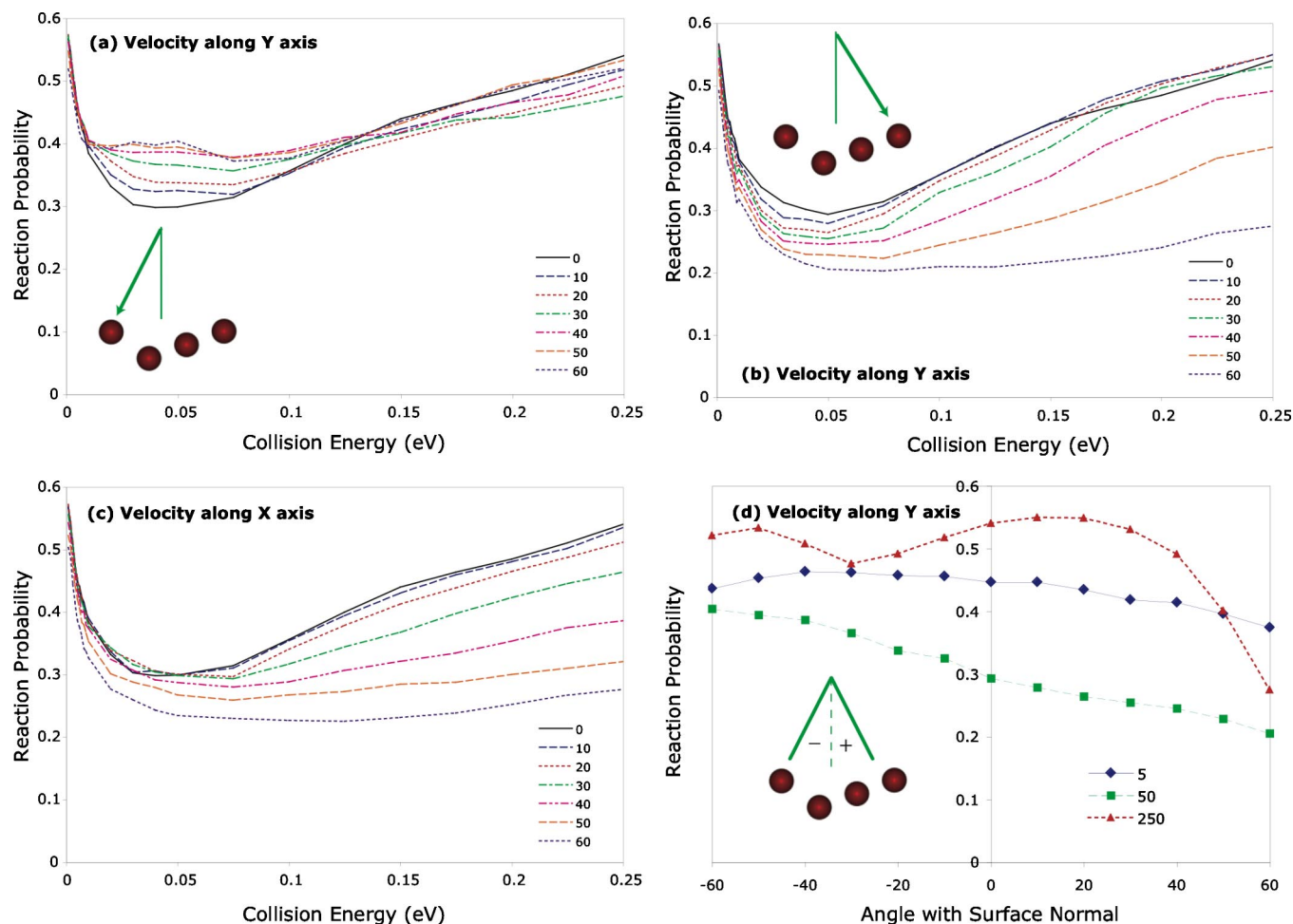
FIG. 3. (Color) Normal and off-normal reaction probabilities. (a) Reaction probabilities for six different angles of incidence, with a parallel component of momentum along the positive Y axis, as indicated by the inset diagram. The angles are indicated in the legend relative to the $-Z$ axis, which is normal to the surface. The collision energy is the initial translational energy of the molecules (not the normal component thereof). (b) As in (a), but with motion along the negative Y axis. (c) As in (a), but with a parallel component of momentum along the X axis, and no component in Y. (d) The angular dependence of reaction for three different initial translational energies: 5, 50, and 250 meV. The legend indicates the translational energies of the three plots. The angle in question is given in degrees, and is relative to the $-Z$ axis. The plots are for incidence with a component of motion along the Y axis. The inset diagram indicates the positive and negative directions.

surface. The upper surface already shows signs that molecules between the top-of-step atoms are being repulsed. This is consistent with the repulsive region of the PES seen above that site in Fig. 2(e). The lower part of the isosurface shows signs of attraction above the top-of-step atoms and above the region where the potential wells are located [Fig. 2(e)].

Figure 4(b) shows the isosurface near the peak of interaction. The isosurface can be seen to extend downwards at the top-of-step atoms, where reaction is occurring. The molecules in the region between the top-of-step atoms have been scattered back, and are returning to the gas phase. At the same time, a second (yellow) isosurface has begun to appear. This isosurface is formed by creating a density of the bond centers of molecules that have reacted at or before a given time. (Reaction is defined to have occurred when the bond length exceeds $4.5a_0$.) The position of any reacted molecule is taken to be the location of the bond center at the point of reaction, and is frozen in space for all future times. Clearly the top-of-step atoms are dominating this reaction. Figure 4(c) is for a time shortly after that of Fig. 4(b), and shows the reacted molecules more clearly.

Figure 4(d) demonstrates that the potential wells seen in Fig. 2(e) cause molecular trapping; the two separate potential wells are even mirrored in the form of the isosurface. Molecules in this "trapping region" may remain there for a considerable amount of time, before reacting or scattering back. Reaction that results from this trapping all ends above the top-of-step atoms—there is no reaction at the site of trapping itself or on the terrace sites. In order to dissociate, molecules in the trapping region migrate to the nonactivated step site.

Figure 5 includes three movies, all for the high collision energy of 0.25 eV. From the frames for normal incidence [Figs. 5(a)–5(d)], it is clear that while reaction is still very much prevalent on the top-of-step atoms, some reaction now occurs above the central terrace atom. Also interesting in Figs. 5(c) and 5(d) is that the molecules scattering from the terrace appear to acquire a component of momentum parallel to the surface, in the +Y direction. This can be established by observing that the green volume corresponding to the scattered molecules in Fig. 5(c), has moved to the left somewhat in Fig. 5(d).

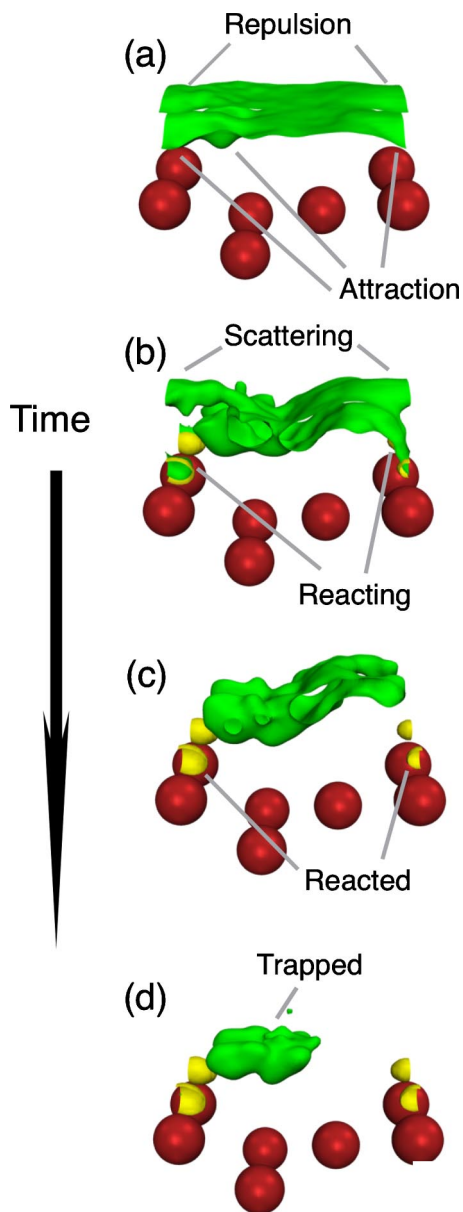Figures 5(e) and 5(f) are for incidence at 60° to the nor-

FIG. 4. (Color) Visualization of dynamics for normal incidence at 5 meV. (a)–(d) Two isosurfaces are shown in each time frame: a green one for the total density of molecules, and a yellow one corresponding to reacted molecules, which are frozen in position at the point of reaction. The four different frames correspond to different times, with time increasing down the page. The frames are not necessarily equally spaced in time. Labels have been added to aid discussion.
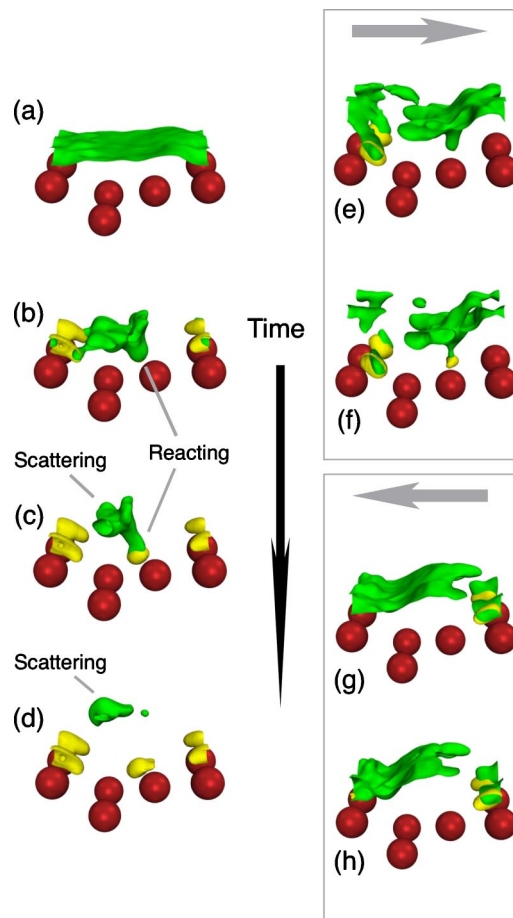

FIG. 5. (Color) Visualization of dynamics for a collision energy of 0.25 eV. (a)–(d) Isosurfaces for the total density of trajectories (green) and reacted density (yellow) for normal incidence at 0.25-eV collision energy. Time increases moving down the page [i.e., from (a) to (d)], with frames not necessarily equally spaced in time. (e) and (f) Isosurfaces for off-normal incidence at 60° to the surface normal parallel to the YZ plane. The arrow indicates that the incident molecules have a component of velocity in the direction of $-Y$. (g) and (h) As for (e) and (f) except that the incident motion has a component in the direction of $+Y$.

mal, with the molecules moving to the right. It is clear from these frames that reaction occurs at the top-of-step atom, though the isosurface for reacted molecules is now more to the side of the atom than directly above it. A closer inspection reveals that the isosurface of unreacted molecules must deform considerably to reach this reactive "hot spot," while avoiding the repulsive terrace. Parts of the isosurface that would otherwise be on a course to react at the top of the step, get "shadowed"[35] from it by repulsive regions of the terrace, and are seen to scatter back in Fig. 5(f). This is evident in the concave form of the isosurface over the terrace, just in front of the top of the step. The terrace itself shows some reaction above the central atom.

Incidence with a component of motion in the $+Y$ direction is covered in Figs. 5(g) and 5(h). In this case there is little or no reaction on the terrace, but reaction readily occurs at the step. It is clear that the passage of the molecules to the reactive top-of-step atom is not hindered by any repulsive region of the PES, as it was in Figs. 5(e) and 5(f). In fact, Fig. 2 shows that the opposite is true: approaching off normally in the $+Y$ direction allows molecules to pass through the potential wells, which form an attractive channel directly to the reactive site [Figs. 2(e), 2(g), and 2(h)]. Evidence of this attraction can be seen in the way that the total density isosurface sinks down in front of the upper step edge.

The effect that shadowing by the terrace has on reaction at the step is evident in the initial envelope of reactive trajectories (Fig. 6). The isosurfaces shown in this figure were created by decomposing the full density (see Appendix A) to form a new density for only those trajectories that eventually react. (In viewing Fig. 6, it should be borne in mind that the trajectories are incident off normally, and the isosurfaces move approximately 1/3 of the length of the unit cell in Y before strong interaction with the surface occurs.) The figure
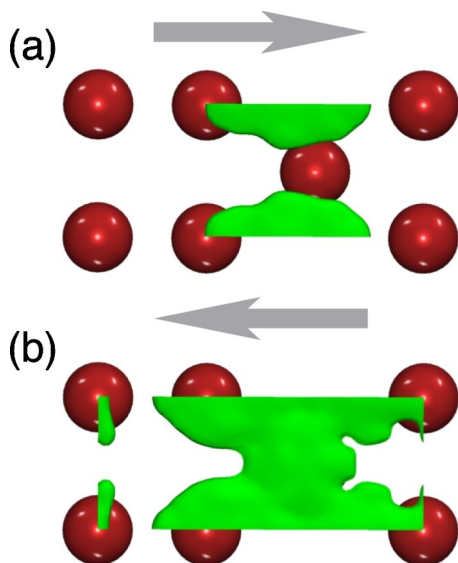
FIG. 6. (Color) Isosurface of the initial density of reacting molecules for off-normal incidence. (a) View from above the unit cell of the isosurface for molecules incident parallel to the YZ plane, with a component of momentum in the $-Y$ direction. (b) As in (a), but for molecules incident with a component of momentum in the $+Y$ direction.
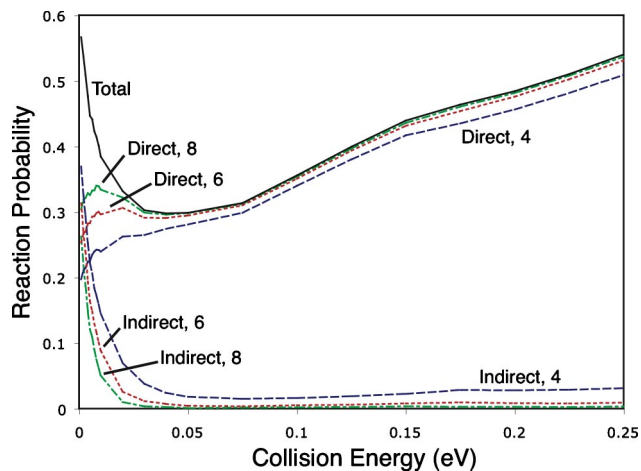

FIG. 7. (Color) Direct and indirect reaction for normal incidence as a function of collision energy. The total reaction probability is given, along with various decompositions into direct and indirect reactions, based on the turning point criterion described in the text. Results are shown for three different values of the turning-point threshold: 4, 6, and 8.

shows that molecules incident with motion in the $+Y$ direction can react from many more positions in the unit cell than those incident with motion in $-Y$. The "window" of reaction is larger when approaching the top of the step via the attractive potential wells than when having to cross the repulsive terrace [Figs. 2(g) and 2(h)]. From Fig. 6(b) it is also clear that molecules do not have to approach the reactive sites directly in order to react: there is a large portion of the density in the center of the cell above the central terrace atom. In order to react, molecules beginning there must be steered sideways in X in order to reach the reactive top-of-step atoms. Figure 2(e) shows that the repulsive ridge of the PES that covers most of the step is well suited to achieving this steering. It is knifelike in character, and thus capable of splitting the incident density, pushing it toward the reactive sites. In contrast, the repulsive region over the terrace forms a wall to molecules incident in the $-Y$ direction, shadowing them from the reactive sites, rather than steering toward them.

These visualizations suggest a metaphor for the PES of the $H_2+Pt(211)$ system: a kitchen sink. The top sites form the reactive plughole, with the potential wells above the lower edge of the step defining a catchment basin. At low energies, trajectories can be caught in the bottom of this basin, and take some time to trickle into the plughole or evaporate back to the vacuum. At high energies, this basin acts to concentrate trajectories in the direction of the reactive plughole. Molecules approaching normal to the surface, or with momentum in the $+Y$ direction, are guided by the basin to the plughole; those approaching from the $-Y$ direction enter the basin on the side closest to the plughole, and are effectively shielded from it.

D. Directness of reaction

The low-energy decline in reaction with collision energy and subsequent increase point to two different contributions.

This could arise from dynamical steering,[10,11] but as we have already seen, trapping in the potential wells observed in Fig. 2 is the likely culprit. One way to extract the trapped component of reaction is to consider how "directly" each trajectory reacts. A measure for this is the number of turning points it undergoes perpendicular to the surface (i.e., in the Z coordinate) before it reacts.[17] Direct reaction is considered to have occurred if the number of turns made is less than a given threshold, with all other trajectories being categorized as indirect.

Figure 7 presents decompositions of the reaction probability at normal incidence, for various values of the turning-point threshold. The choice of threshold is somewhat subjective, but it is clear that choosing a value of 8 results in a direct component that rises with decreasing energy at low energies, and a value of 4 prevents the indirect component from dropping to zero at high energies. A threshold of 6 represents a reasonable compromise in which the direct reaction increases monotonically with energy, and the indirect component decreases monotonically to practically zero. We will thus consider direct reaction to involve less than 6 turning points in Z.

The direct component of reaction does not decrease to zero at low energies in Fig. 7. It begins at around 0.25, and rises with collision energy, as a wider range of impact geometries and surface sites become reactive, including sites with an activation barrier such as the terrace.

The indirect component decreases with collision energy. A molecule entering the potential wells undergoes an internal transfer of energy, from motion along the surface normal (Z) to other degrees of freedom. Because there is so little translational energy to begin with, the motion of the molecule away from surface is insufficient to exit the well and escape. The molecule is trapped, and has a heightened probability of migrating to the top of the step and reacting [Fig. 2(e)]. The greater the incident energy, the more likely the molecule will be able to escape the wells before reacting, and the less probable the molecule will react via the indirect channel.

E. The nature of trapping

It is worth devoting some time to the nature of the potential wells seen in Fig. 2(e), and the trapping that occurs within them. The wells in question are very shallow (34 and 124 meV), not much deeper, if any, than a physisorption well. But the wells in question are most certainly molecular chemisorption wells, not least because the level of DFT used to calculate the PES is incapable of treating physisorption. The proximity of the wells to the surface also points to a chemical bond. Andersson and co-workers have reported experimental and theoretical results for a similar molecular chemisorption well for H_2 interacting with a Cu(510) surface.[36]

One question that may reasonably be asked is whether trapping would persist in quantum-mechanical calculations. Other studies suggest that where trapping arises classically, it also tends to occur in the quantum system, though details inevitably vary.[18] An often-used approach to assessing the likelihood of quantum trapping involves estimating the ZPE of the trapping well, and comparing it to the gas phase value. Using harmonic normal-mode analysis, we have calculated the ZPEs for motion in each well. The ZPE of the molecular vibration drops from 269 meV in the gas phase to 267 meV in the shallow well, and 254 meV in the deep well. Other modes of oscillation increase to more than compensate for these drops, leaving the shallow well with a total ZPE of 320 meV, and the deep well with 357 meV. Subtracting the change in ZPE from the well depths results in ZPE-adjusted well depths of −17 and 36 meV, for the shallow and deep wells, respectively. In other words, this simple analysis suggests that the shallow well will cease to exist from the perspective of quantum dynamics, and the deep well will be considerably shallower.

Many aspects of this assessment are questionable, and probably the only way to be sure if trapping would really arise quantally is to actually perform quantum-mechanical calculations. The normal-mode analysis may give reasonable values for the strongly oscillatory, and reasonably harmonic bond-stretch vibrational mode, but ZPEs of weakly frustrated rotations and translations are likely to be overestimated due to their intrinsic anharmonicity. The true ZPE of the wells could lie considerably lower. The relevance of such comparisons is also cast into doubt by findings that changes in ZPE are often compensated by the quantum-mechanical system in other ways.[11]

Trapping in the quantum system could even be more effective than it is classically, greatly favoring reaction. The quantum density of states for escape from the trapping wells to the gas phase is considerably smaller at low energies than the classical density of states. This is evident when one considers that at a collision energy of 1 meV, the only scattering states energetically open to the quantum system are the elastic channel, and two singly excited diffraction states. No vibrational, rotational, or x-diffractional excitation is quantally possible. The classical system is not restricted in this way, and can distribute energy into any of its degrees of freedom, increasing the pathways it has to escape the well and scatter back to the gas phase. This reasoning suggests that quantum-

TABLE I. First-order rate coefficients for escape from the trapping region defined in the text. Results are given for different collision energies at normal incidence, and for the two separate product channels, along with the overall (total) rate constant for product formation. The procedure for calculating the table is explained in the text. The unit of the rate coefficients is ps^{-1}.

Collision energy (meV)	Product channel		
	Reaction	Scattering	Total
1	0.77	0.47	1.12
5	0.95	1.04	1.96
9	1.32	1.88	3.19

mechanical calculations may well predict that trapping is even more effective than we predict here, and result in more reaction at low energies.

Because the internal degrees of freedom of trapped molecules are reasonably equilibrated, it is possible to consider trapping from a statistical viewpoint. The population of the trapping region decays approximately exponentially in time, and this decay can be represented by a first-order rate coefficient. The decay can also be decomposed into contributions for the two product channels, dissociation and backscattering, and rate coefficients calculated for each channel separately.

Table I gives rate coefficients for escaping the trapping region at three different incidence energies. For this purpose, the trapping region was simply defined as a rectangular prism running parallel to the X axis, with Y in the range of $[5.0a_0, 10.5a_0]$ and Z in the range of $[2.5a_0, 5.5a_0]$. Any molecule inside this volume—after accounting for periodic boundary conditions—was considered to be in the trapping region. The rate coefficient for the respective product channels are here defined as

$$\frac{dP_c(t)}{dt} = -k_c(t)P_{tot}(t), \tag{3}$$

with $P_c(t)$ the population of trajectories in the trapping region at time t that ends in product channel c, $P_{tot}(t)$ the total number of trajectories in the trapping region at time t, and $k_c(t)$ the rate coefficient. The rate coefficients $k_c(t)$ are not constant, but can be assigned an instantaneous value for a given time. To do this, we first evaluated rate constants for the decay of the various $P_c(t)$ using linear fits to semilog plots of P_c vs t, up to a time of 100 000 a.u. The rate coefficents $k_c(t)$ were then estimated for a time of 10 000 a.u. by dividing the rate constants by $P_{tot}(t=10\,000$ a.u.). This gives in indication of the rate product formation in each channel early in the reaction.

Table I shows that for 1 meV, the rate of decay for the reaction channel is considerably higher than for scattering, indicating a propensity for trapped molecules to react. As energy is increased, the scattering rate coefficient increases in relation to that for reaction, surpassing it even at 5 meV. As energy is increased and the scattering channel "opens up," relatively more trapped molecules scatter back to the gas phase. All rate coefficients increase with energy, including the total rate constant, which is indicative of a decrease
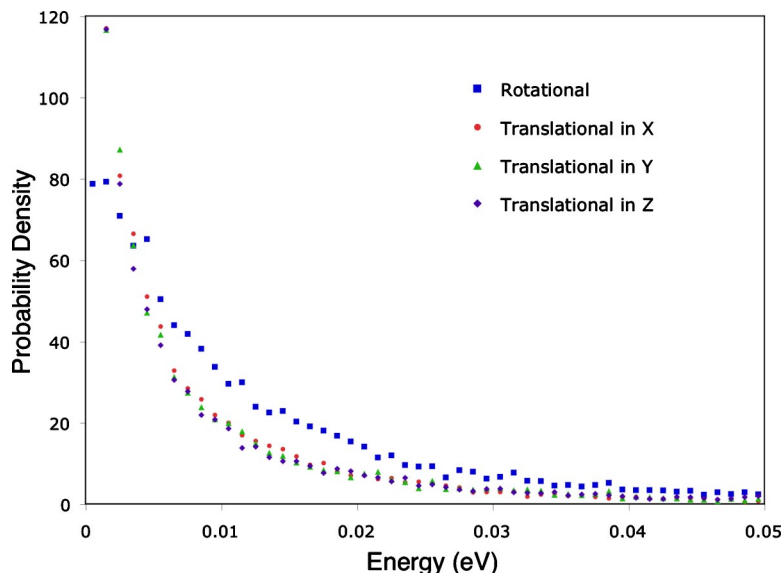
FIG. 8. (Color) Kinetic-energy distributions of trapped molecules at 20 000 a.u. of time. Plots are for rotational kinetic energy and three components of translational motion, in the X, Y, and Z coordinates. Results are for a total ensemble of 100 000 trajectories initiated with 5 meV of collision energy normal to the surface.

in the lifetime of trapped molecules. As can be seen in Fig. 7, very little trapping persists above about 30 meV.

We have now described the static PES giving rise to trapping and statistical aspects of the trapping, but we have yet to address what actually causes molecules to become trapped. Molecules entering the wells in the PES always have enough total energy to escape, so why do they become trapped in the first place? The trapping arises due to a dynamical effect: energy initially concentrated in motion toward the surface is internally redistributed to other degrees of freedom in the trapping region, leaving too little energy in the motion away from the surface for escape. But what are the internal degrees of freedom involved in this energy dissipation?

Figure 8 gives the probability distributions for different components of the kinetic energy of molecules in the trapping region at a fixed point in time (20 000 a.u.). The vibrational energy is not included, because it remains virtually zero. Rotational degrees of freedom are clearly excited in the well, as are parallel translations. For the time shown, the translational degrees of freedom have almost equilibrated with one another, such that motion for X and Y is indistinguishable energetically from that for Z, in which all the kinetic energy is initially concentrated. Summing the translational components, it is clear that more energy exists in translation than in rotation, but that a significant amount is present in both types of motion. The average value of rotational kinetic energy is 13.3 meV, and for translation it is 22.5 meV. These results demonstrate that trapping comes about due to a transfer of energy out of motion in the scattering coordinate, and into parallel translational and rotational degrees of freedom.

The final aspect of trapping that we consider is mobility. How mobile are the trapped molecules? Can they move from one unit cell to the next? To answer these questions, we present Fig. 9, which shows the diffusion of indirectly reacting molecules in X and Y. (Note that Fig. 9 does not show diffusion relative to absolute positions on the surface, but a distribution of distances traveled by molecules in X and Y from initial position to point of reaction.) Even for the very

low energy used (1 meV), diffusion between unit cells is possible in the X direction, though diffusion along Y is constrained to a single cell.

The peak of the distribution that appears with X and Y areapproximately 1.0 and 6.0, respectively. Indirect molecules tend to begin in and around the trapping wells, so they need to move some distance in the $+Y$ direction to get to the reactive step, and a small distance in X. What is perhaps
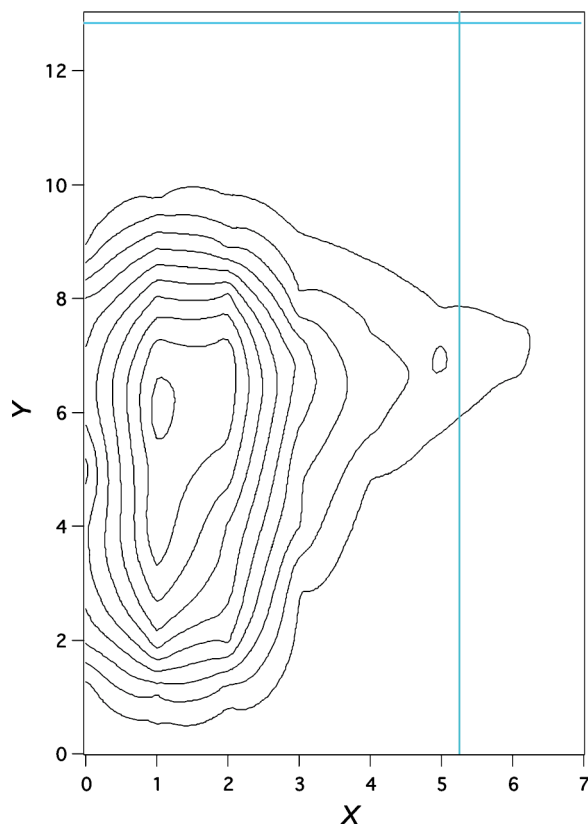

FIG. 9. (Color) Diffusion of indirectly reacting molecules incident normal to the surface at 1-meV collision energy. The contour plot shows the distribution of the distance moved in X and Y by indirectly reacting molecules. Distances are given in bohr. The lines delineate the width and length of the unit cell.

more interesting is that molecules often move much further in X than is strictly necessary into a neighboring cell. This is indicated by the broadness of the distribution in X, and suggests that molecules are reasonably mobile in the X direction, even at very low energies. Contour plots of the PES show transition states between different halves of the unit cell [Fig. 2(f)] and neighboring unit cells [Fig. 2(h)], which are below the gas phase minimum, and thus conducive to migration in X. The same is not true of Y, where considerable barriers to diffusion exist on the terrace sites [Figs. 2(f)–2(h)].

F. Site dependence of reaction

The experimental findings of Hayden and co-workers,[5,6] along with the visualizations of Fig. 5, suggest that there are distinct contributions to reaction from sites on the step and terrace. To quantify this, Fig. 10 gives site-dependent decompositions of the reaction. The terrace has been defined as that part of the unit cell with Y in the range of $[2.0a_0, 8.0a_0]$. Any reacting trajectory terminating in this region, after appropriate mapping to account for periodic boundary conditions, is deemed to have undergone terrace reaction. The remaining reacting trajectories are associated with the step.

Figures 10(a) and 10(b) show that below about 50 meV, there is no reaction on the terrace. This is consistent with the terrace sites exhibiting an activation barrier [Fig. 2(c)]. The step reaction curves below 50 meV are thus reminiscent of those for the total reaction probability (Fig. 3). Above 50 meV, the terrace site exhibits monotonically increasing reaction.

From Figs. 10(a) and 10(b), it is clear that reaction at the step is most favorable with the molecule approaching in the $+Y$ direction at very off-normal incidence. The most reaction at high energies is seen to occur at the maximum angle shown of 60°. We were able to explain this above with reference to the visualizations in Fig. 5 and the PES plots in Fig. 2. Figures 2(f)–2(h) show that molecules incident with a significant component of velocity in the $+Y$ direction encounter far less repulsion than when those incident from other directions, because they can travel along the channel formed by the potential wells. Molecules moving in the $-Y$ direction are shadowed from the reactive step sites by the repulsive terrace. These attributes of the PES lead to the asymmetry observed in reaction on the step site at high energies.

Figures 10(a) and 10(b) show that reaction on the terrace is greatest for incidence angles corresponding closely to the normal vector of the terrace itself. The greatest reaction is seen for the curve corresponding to incidence at 30° in the $-Y$ direction [Fig. 10(b)]. The terrace normal vector makes an angle of 19.45° with the surface normal. For incidence on either side of the terrace normal, reaction decreases, as can be more clearly seen in Fig. 10(c).

The probabilities for reaction on the terrace in Fig. 10 may seem low when compared to experimental[37,38] and theoretical studies[39] of Pt(111); however, in order to make such a comparison, the probabilities given in Fig. 10 need to be adjusted to account for the surface area associated with the Pt(111) surface, as well as the fact that the surface normal of
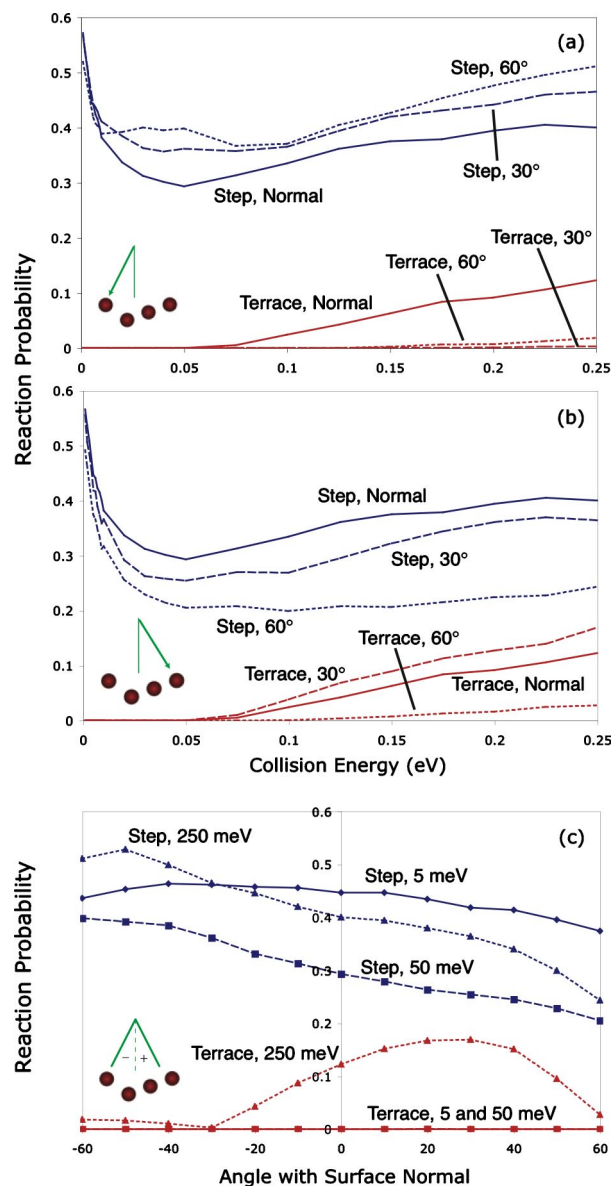

FIG. 10. (Color) Decomposition of the reaction probability into step and terrace contributions. The step and terrace regions are defined in the text. (a) Reaction probability curves, decomposed with respect to reaction site, for angles of incidence giving a component of velocity in the $+Y$ direction, with no motion in X. (b) As in (a), except that molecules are incident with a component of momentum in the $-Y$ direction. (c) Decomposed reaction curves as a function of incidence angle, with no component of initial velocity directed along the X axis. Each curve is for a different combination of reaction site and collision energy. The inset diagram indicates the convention chosen for positive and negative angles of incidence.

the terrace does not correspond to that of the Pt(211) surface. When these adjustments are made, the reaction probability for molecules incident on the Pt(111) terrace is approximately twice as large as it is in Fig. 10, in line with other studies.

The angular dependencies of reaction shown in Fig. 10(c) confirm that reaction is comprised of two relatively independent contributions. At low energies (e.g., 5 meV), total-energy scaling is obeyed, with all reactions ending at the step site. At these energies, there is a significant indirect component, which does not have a strong dependence on incident angle: molecules become trapped, and quickly lose
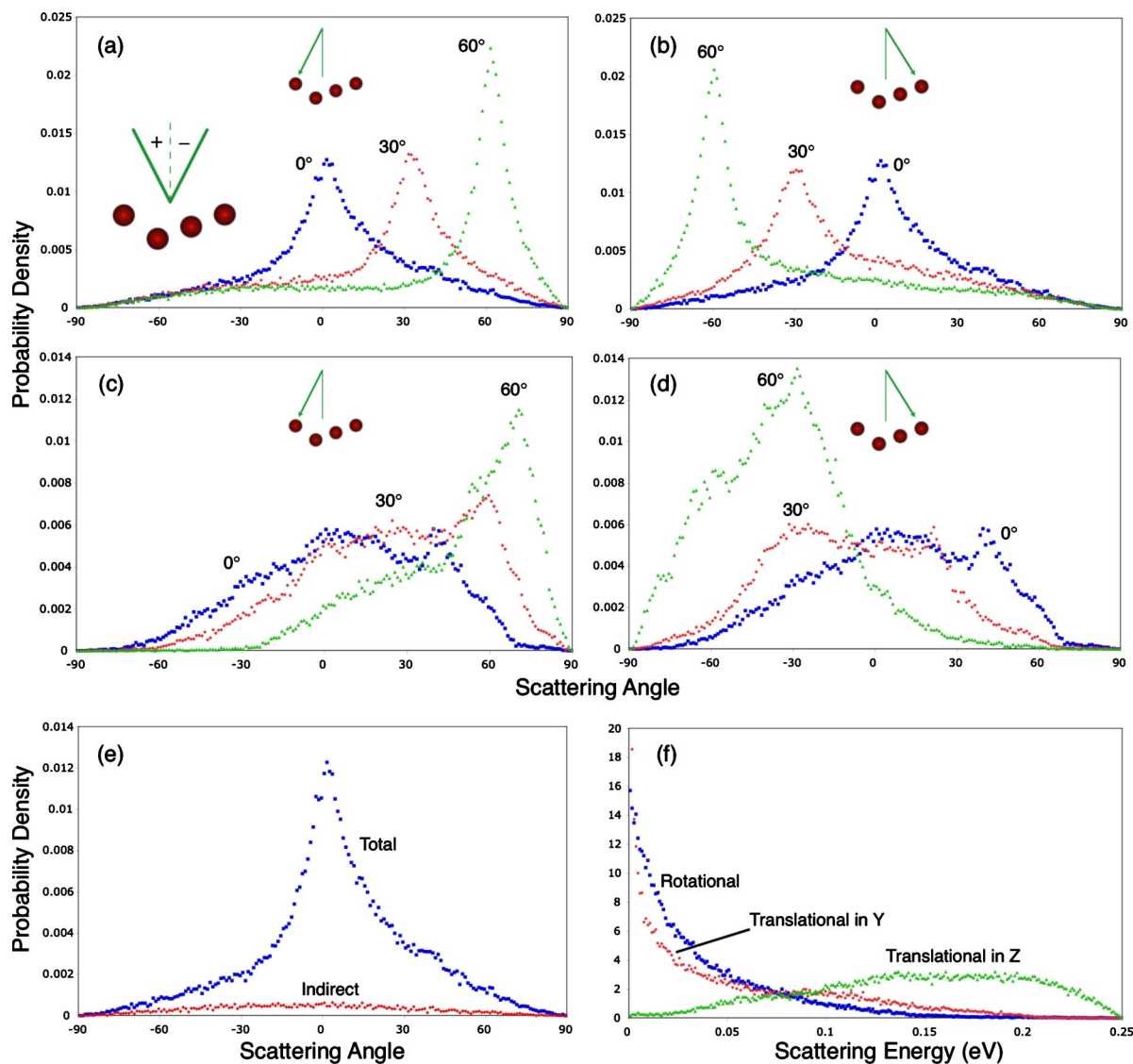
FIG. 11. (Color) Properties of scattered molecules. (a) The scattering angle distribution taken in the YZ plane for different angles of incidence at 5 meV of collision energy. Plots are labeled according to the angle of incidence with respect to the surface normal. Molecules approach parallel to the YZ plane, with a component of velocity in the direction of the $+Y$ axis. An inset diagram indicates the sign convention for scattering angles, and another the direction of incidence with respect to the Y axis. The results are based on an ensemble of 100 000 trajectories. (b) As in (a), but for molecules with an incident component of velocity in the $-Y$ direction. (c) As in (a), but for a collision energy of 0.25 eV. (d) As in (c), but for molecules with an incident component of velocity in the $-Y$ direction. (e) The total angular scattering probability distribution and that of indirect trajectories, for normal incidence at 5-meV collision energy. (f) Scattering energy probability distributions for molecules normally incident at 0.25 eV. Plots are given for the translational energy in Z, the translational energy in Y, and the rotational energy.

all memory of their initial direction of travel. Increasing to 50 meV, indirect reaction has virtually dropped to zero, and there is a clear preference for reaction of molecules with parallel translational motion in the $+Y$ direction. This is again the effect in which molecules reacting at the step can pass unimpeded through the channel formed by the potential wells.

Terrace reaction is only significant in Fig. 10(c) at 250 meV. It has a peaked form, with maximum reaction near— but not exactly equal to—the angle corresponding to the terrace normal. Note that the form of the curve is not symmetric, so normal energy scaling cannot be said to apply. The small amount of reaction seen at large negative angles has been traced to reacting molecules from the step site being carried into the terrace region by the large component of

parallel momentum they possess. It is thus an artifact of the simple scheme used to partition step from terrace, and should be ignored.

G. Scattering distributions

Scattering angle distributions are shown for different incidence angles and collision energies in Fig. 11. At 5 meV [Figs. 11(a) and 11(b)], the distributions are strongly peaked at the angle for specular reflection. At such low energies, most molecules do not approach close enough to the surface to sample significant corrugation, and thus scatter elastically. The peak increases in height as the incidence angle is increased in either direction, because the reduction in normal energy resulting leads the molecules to sample even less cor-

rugation. The scattering distribution at normal incidence exhibits a broader shoulder for scattering in the $+Y$ direction [Figs. 11(a), 11(b), and 11(e)]; we have been able to trace this to direct reflection of molecules from the terrace. The angle made by the terrace with the Y axis (19.45°) means that molecules elastically reflecting from the terrace are imparted a component of velocity in the $+Y$ direction.

At high energies [Figs. 11(c) and 11(d)], the terrace reflection is even more evident, in the form of a sharp peak. [This peak also shows up very slightly in the plots for 5 meV (Figs. 11(a) and 11(b)).] The peaks increase in magnitude as molecules approach the terrace at more acute angles. This is because reaction on the terrace decreases for more off-normal incidence, and scattering thus increases. The peaks fall very close to the angle corresponding to elastic reflection from the terrace; for molecules incident normal to surface, for example, the peak appears at around 40°, approximately twice the angle made by the terrace normal with the surface normal (i.e., 19.45°).

The remaining scattering at high energies is peaked at the elastic reflection angle of the surface [Figs. 11(c) and 11(d)], but is considerably broader than seen for low energies [Figs. 11(a) and 11(b)]. This is consistent with the molecules sampling a greater corrugation, as they approach closer to the surface.

Figure 11(e) compares the total probability distribution for normal incidence at 5-meV collision energy, with the contribution due to indirect trajectories (corresponding to trapped molecules). The total distribution is much more strongly peaked, with the indirect scattering smeared out over the whole range of scattering angles. The trapped molecules undergo considerable energy exchange between different internal degrees of freedom, as shown in Fig. 8, effectively losing all memory of their original direction of motion. We have determined that the maximum indirect scattering occurs for an incidence energy of around 5 meV. At this energy, approximately 5% of all trajectories undergo trapping and subsequent scattering. It may be possible to measure this population experimentally, and doing so would support our findings that the reaction at low energies is influenced by molecular trapping.

One may question whether or not the angular distributions shown for low energies have any bearing on quantum-mechanical diffraction. In some instances, it is possible for a classical system to exhibit inelastic diffractive scattering when it is quantum mechanically forbidden. In this instance, that is not the case, because the unit cell is particularly long in Y, reducing the energy required to excite diffractional states. The first diffractional state for Y is at 0.887 meV, and the second at 3.55 meV. At 5 meV it is thus possible to excite by two quanta, and some measure of the scattering effects seen here should be possible to establish experimentally.

Scattering energy distributions of molecules normally incident at 0.25 eV are shown in Fig. 11(f). The translational motion in Z, which initially contains all of the kinetic energy, exhibits a broad distribution of energies, which tapers off at 0.25 eV. There is clearly excitation of rotational and parallel translational degrees of freedom, but the plot for translational
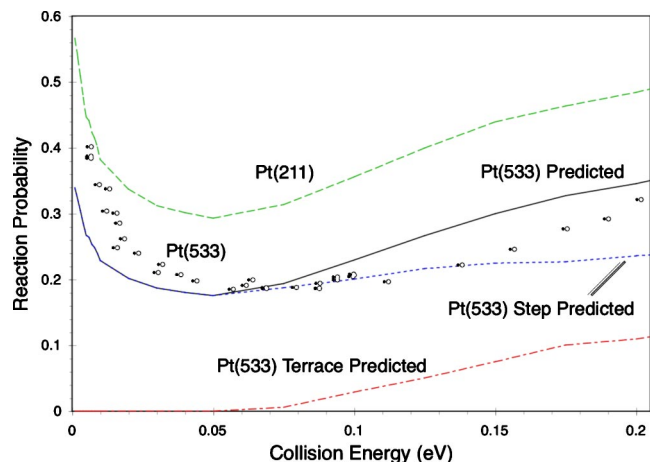

FIG. 12. (Color) Comparison of reaction probabilities with experimental results for Pt(533) (Refs. 5 and 6). The results of Hayden and co-workers (Ref. 5) are shown as circles. The curves calculated in this study are given as lines. The reaction probability calculated here for normal incidence on Pt(211) is shown, along with an estimate of the reaction of Pt(533) based on our calculations for Pt(211). The details of this estimate are given in the text. Plots are also shown for the estimated components of step and terrace reaction on Pt(533), based on our results for Pt(211).

energy in Y is broader than that for rotational energy, indicating stronger coupling between translations in Y and Z than between rotation and normal translation.

H. Comparison with experiment

Hayden and co-workers have recently performed experiments for reaction of H_2/D_2 on Pt(533),[5,6] a system that is very similar to the title reaction here. The Pt(533) stepped surface is virtually the same as the Pt(211) surface, with the exception that the Pt(111) terrace is one row of atoms wider. It is thus quite reasonable to compare results for the two systems, and use the theoretical results for Pt(211) to help interpret the experimental findings.

Figure 12 compares the reaction probabilities determined by the experimentalists at normal incidence,[5] with our results for Pt(211), and reaction curves based on the results for Pt(211) that have been crudely adjusted to account for the longer terrace of Pt(533). The adjusted reaction probabilities are given by the following formulas:

$$P_{step}^{(533)} = P_{step}^{(211)} \frac{L_Y^{(211)}}{L_Y^{(533)}}, \tag{4a}$$

$$P_{terrace}^{(533)} = 2P_{terrace}^{(211)} \frac{L_Y^{(211)}}{L_Y^{(533)}}, \tag{4b}$$

$$P_{total}^{(533)} = P_{step}^{(533)} + P_{terrace}^{(533)}, \tag{4c}$$

where each probability is labeled by the surface (i.e., 211 or 533) and a region of the surface (i.e., step, terrace, or total). Lattice constants for the Y coordinate are represented by L_Y, and are also labeled by the surface type. These simple equations assume that reaction at the step site will be the same for Pt(211) and Pt(533), and that the amount of terrace reaction per unit cell will be twice as great for Pt(533), because the terrace of Pt(533) has two reactive sites and Pt(211) has just

one. Each probability for Pt(211) is also adjusted by the ratio of the lattice constants, to account for the difference in density of molecules in the different unit cells.

Figure 12 shows remarkably good agreement between our predictions for Pt(533) and the experimental findings. The Pt(533) reaction curve derived from our calculations is considerably lower than for Pt(211). This is because the reactive step sites occupy a relatively smaller area of Pt(533) than Pt(211), meaning less molecules are incident at the step on Pt(533).

The poorest agreement between the calculated and experimentally determined probabilities in Fig. 12 is at low energies. The experimental probability increases considerably more than the prediction. There could be a number of reasons for this. First, our PES cannot account for physisorption, and so may underestimate the effect of trapping. Second, as discussed earlier, the density of states for molecules escaping the trapping wells and scattering back to the gas phase is classically greater than it is quantally. A quantum calculation may thus predict significantly more reaction due to trapping at low energies.

Despite these discrepancies, our results appear to give a qualitatively correct picture of the reaction, even if not quantitatively accurate at all energies. This suggests that the mechanisms that we have uncovered in the classical trajectory calculations could provide insight into the experimental results, and we thus move on to assessing the interpretations given to the experimental findings.[5,6]

With the limited information available to them, Gee *et al.* tentatively inferred that reaction on Pt(533) could be broken into four components:[5]

(1)   A temperature-dependent component active at very low energies ($<$30 meV).[6] This was attributed to a conventional molecular physisorption precursor.

(2)   A direct component attributed to reaction on the terrace. According to the authors, this monotonically increasing component dominated reaction at high energies.

(3)   A small component of direct reaction at the step at high energies. This was suggested to contribute only around 17% of reaction for normal incidence at 180 meV, although it increased significantly for off-normal incidence, and was estimated to peak for molecules approaching parallel to the terrace.

(4)   A temperature-independent indirect component terminating at the step, which decreased with energy up to a maximum of around 150 meV. The authors could not determine the mechanism responsible for this component, though they could confidently rule out dynamical steering.

Many of our findings here are in good agreement with the inferences of Gee *et al.* We also find an indirect component of reaction, like (1) above, that decreases with collision energy and scales with total energy. In our calculations, it arises from trapping in weak chemisorption wells, rather than a physisorption well, but the effect is similar. We would expect molecules trapped in the chemisorption wells to exchange energy with the surface,[14] and thus show a temperature dependence as was seen in the experiment. We cannot

rule out the existence of physisorption, because the current state of the art DFT functionals used to create the PES in this study cannot accurately model physisorption wells; however, it is clear that mechanisms other than physisorption, like the chemisorption seen here, could also explain the experimental measurements.

Direct reaction at the terrace (2) is also seen in this study at high energies, and is similarly peaked for incidence normal to the terrace. However, we estimate the terrace contribution to reaction to be considerably smaller than predicted by Hayden and co-workers.[5,6] They assume that nearly all reaction at high energies and normal incidence occurs on the terrace sites, but Fig. 12 suggests that the terrace contributes only around a third of the total reaction on Pt(533) at 0.20 eV. Our results would suggest that the fit used by the experimentalists (Fig. 3 of Ref. 5) overestimates the contribution of terrace reaction, and thus underestimates the role played by the step. Gee *et al.* infer the existence of direct reaction at the step, but only for high energies. They find this component to have a highly asymmetric dependence on incidence angle, in line with our findings here, but have likely underestimated its magnitude.

The final contribution to reaction acknowledged by Gee *et al.* is the temperature-independent indirect component that decreases with energy (4). The exact mechanism of this component could not be established. In this study, we have not come across any component of reaction with these characteristics, and suggest that it is likely an artifact of the fitting procedures used in the experimental analysis, in particular, the assumption that reaction at high energy can be almost entirely attributed to the terrace sites. The temperature-independent indirect component probably arises when terrace reaction is overestimated at high energies and direct reaction at the step neglected at low energies.

Gee *et al.* appear to have made the assumption that the step sites of Pt(533) would have an activation barrier.[5] Our DFT calculations suggest that this is unlikely, predicting that above the top-edge step atoms the potential is highly attractive, with no barrier (Fig. 2). It is unlikely that these calculations would be so severely in error that an activation barrier could arise. (The low coordination of the top-of-step atoms also lends credence to the existence of nonactivated sites at the step.) If we assume that the step is nonactivated, then there will be direct reaction there at all energies, and a significant contribution at high energies. This is supported by the dynamics presented here, and can easily be reconciled with the experimental data of Refs. 5 and 6.

IV. CONCLUSIONS

In this study, we have performed the first extensive study of reaction dynamics of a molecule on a stepped surface with a DFT PES. The dissociative adsorption of H_2 on Pt(211) has been studied with the aid of classical trajectory calculations in order to determine reaction probabilities and scattering angle distributions. Techniques have also been developed to visualize the reaction, and analyze aspects of the trajectories that are not directly observable by experiment. This offers

much greater insight into the mechanisms involved than simply gathering data for observables, and using it to infer the dynamical mechanisms.

The PES developed for H_2 reaction on Pt(211) was based on around 10 000 energy points calculated with DFT at the GGA level. A high-quality interpolation of the DFT/GGA data was performed using the corrugation reduction procedure.[20,24] The PES exhibits nonactivated sites above the top-of-step atoms, where reaction can occur spontaneously. The terrace sites are repulsive, exhibiting barriers, though above the central terrace atom, the barrier to reaction is quite low (approximately 50 meV). A region exists above the lower edge of the step that includes two shallow chemisorption wells, 34 and 124 meV deep (relative to the gas phase minimum). These wells play an important role in reaction at all energies.

Reaction probability curves show the characteristic nonmonotonic dependence on energy seen in most nonactivated systems. The inverse dependence of reaction at low energies was shown to arise from trapping in the chemisorption wells above the lower edge of the step. The initial translational energy perpendicular to the surface is redistributed to parallel translational and rotational degrees of freedom, leaving molecules with too little energy in the motion away from the surface to break the attraction of the surface. Trapped molecules have an enhanced probability of migrating to the reactive top edge of the step at low energies. Increasing the collision energy resulted in decreased trapping, and thus decreasing reaction. Superimposed on this indirect component of reaction were two monotonically increasing sources of direct reaction: one nonactivated component, occurring at all energies above the top-of-step atoms, and one activated component, occurring at the terrace from approximately 50 meV upwards.

At off-normal incidence, there was little dependence of reaction on angle of incidence at low energies (<20 meV). To a good approximation, total-energy scaling was obeyed, which is consistent with molecules becoming trapped and "losing memory" of their initial state. At intermediate energies (approximately 30-100 meV), reaction was highly asymmetric for incidence perpendicular to the steps, decreasing approximately linearly with incidence angle. Reaction strongly favored molecules approaching the top-of-step atoms from the step side, rather than the terrace side. This was attributed to two effects:

(1) A hindering of reaction when approaching from the terrace side due to shadowing of the reaction site by repulsive regions of the terrace; and

(2) enhancement of reaction on the step side due to the existence of potential wells, which form an attractive channel favorable to molecules approaching parallel to the terrace.

The angular dependence of the terrace reaction seen at energies above around 50 meV was peaked for molecules incident normal to the terrace, and decreased for incidence away from this direction. This is consistent with an activated reaction and reaction on Pt(111), in particular.[5,37]

Scattering angle distributions for normal incidence were very peaked at low energies, due to the low corrugation of the surface sampled. In contrast to the overall distribution, the angular distribution of molecules escaping after being trapped was very broad, consistent with the view that the internal degrees of freedom of trapped molecules equilibrate and the molecule "forgets" its initial direction of motion. This broad distribution of scattered molecules could represent an experimental signature for the trapping predicted here. For high energies, a distinct peak existed in the scattering angle distributions that corresponded to reflection from the terrace. High-energy distributions were broader in general, due to the increased corrugation sampled by the molecules.

A comparison between our results and the experimental results of Hayden and co-workers for Pt(533) (Refs. 5 and 6) were generally very promising. Reaction probabilities were comparable when adjusted for the larger terrace of the (533) surface, although our results do not quantitatively reproduce the experimental data at low energies. Other aspects of the experimental data were also reproduced by our classical trajectory study, including the nonmonotonic dependence of reaction on energy, the total-energy scaling at low energies, and the strong asymmetry in off-normal reaction at high energies. The ability of classical trajectory calculations to reproduce qualitative aspects of the reaction suggests that the reaction mechanisms presented here are most likely responsible for the experimental observations on Pt(533).

The extra information afforded by DFT and dynamics calculations has enabled us to revisit some of the inferences made in the experimental analyses of Hayden and co-workers.[5,6] We conclude that many aspects of their findings agree well with our study. Our results do suggest that the experimental analysis underestimated the amount of direct reaction at the top of the step and overestimated reaction on the terrace at high energies. Accounting for these discrepancies alleviates the need for a temperature-independent indirect component of reaction that was inferred in the experimental studies.

ACKNOWLEDGMENT

APPENDIX A: VISUALIZATION OF COLLECTIVE CLASSICAL DYNAMICS

Visualization is commonly used with classical dynamics to follow the time evolution of individual trajectories. "Ball-and-stick" models of "representative" trajectories aid in better understanding the dynamics of the whole trajectory ensemble. This approach can be very useful, but the problem of finding truly representative trajectories is not trivial, and inductively drawing conclusions about the many, from observations of the few, is fraught with danger.

The visualization techniques that we have developed for this study are collective in nature. They are used to consider the behavior of all trajectories at once. In this respect they

are more akin to visualizations of quantum wave packets: the time dependence of a density is visualized, rather than a single path.

In order to collectively visualize classical trajectories as a density changing in time, it is first necessary to develop a scheme that fits the discrete classical states in order to form a continuous wavelike density. For this, we use a technique known in the visualization community as "splatting."[40] In effect, the density is represented as follows:

$$\rho(\mathbf{x},t) = \frac{1}{N(t)} \sum_{i=1}^{N(t)} g[\mathbf{x};\mathbf{x}_i(t)], \tag{A1}$$

where $\rho(\mathbf{x},t)$ is the density at time t and point $\mathbf{x}$ in space, $N(t)$ is the total number of discrete trajectories existing at time t, $g(\mathbf{x};\mathbf{x}_0)$ is a spatially normalized function localized around the point $\mathbf{x}_0$, and $\mathbf{x}_i(t)$ is the spatial location of classical trajectory i at time t. In this study, a Gaussian form has been used for $g(\mathbf{x};\mathbf{x}_0)$:

$$g(\mathbf{x};\mathbf{x}_0) = \xi\sqrt{\pi}e^{-\frac{1}{\xi^2}(\mathbf{x}-\mathbf{x}_0)^2}. \tag{A2}$$

One question that immediately arises is "what is the spatial location of a classical trajectory?" A classical trajectory generally exists in a many-dimensional space, not a three-dimensional (3D) one. Before interpolating trajectories to form a continuous spatial density, it is thus necessary to define a "locator," which is a function that maps the coordinates of a classical trajectory to the 3D space:

$$\mathbf{x}_i = L(\mathbf{q}_i), \tag{A3}$$

with $\mathbf{q}_i = [\mathbf{x}_i^{(1)}, \mathbf{x}_i^{(2)}, \ldots, \mathbf{x}_i^{(N)}]$, $\mathbf{x}_i^{(j)}$ being the position of atom j in trajectory i, and $L(\mathbf{q})$ the locator function. The locator used in this paper is simply the center of mass of the molecule, though other possibilities, such as the position of a single atom or center of a bond, could also be appropriate depending on the application.

Once a continuous density has been formed, its time dependence can be visualized. Visualization of scalar fields can take many forms; we have opted in this study to use a contour of the density, which in 3D forms a 2D isosurface. In order to create a visual representation of an isosurface, the density can be evaluated on a regular 3D grid, and then fed into visualization software like the Visualization Toolkit[40,41] (VTK) or OPENDX.[42] (These libraries are freely available, cross platform, and open source.)

When studying surface reactions, with all trajectories initially in a 2D plane parallel to the surface, the density as evaluated above will have a finite width due to the fitting scheme. An isosurface thus appears as two surfaces in the unit cell, rather than one. This effect can be reduced by using narrower fitting functions, but this necessitates more trajectories in order to obtain a smoothly varying density without artifacts. In the limit of infinitely many trajectories it is possible to reduce the fitting functions to zero width, at which point the two isosurfaces will merge into one; of course, in practice this is never realized.

The scheme outlined above can be expanded upon slightly to form a much more powerful visualization approach. Instead of only considering the total density of tra-

jectories, it is possible to classify each trajectory at each point of time, assigning a weight. This makes it possible to decompose the density or generate new densities based on dynamical quantities.

In this more general scheme, the scalar field is expanded as

$$\rho_g(\mathbf{x},t) = \frac{1}{N(t)} \sum_{i=1}^{N(t)} c[\mathbf{q}_i(t'),\mathbf{p}_i(t'),t]g[\mathbf{x};\mathbf{x}_i(t)], \tag{A4}$$

where c will be referred to here as the "classification functional," and ρ_g is now a generalized scalar field, which need not be normalized. In the most general case, the classification functional depends upon the full path of the classical trajectory through phase space. Time-dependent expectation-value fields of the classification functional can be generated by simply dividing by the total density:

$$\rho_{\exp}(\mathbf{x},t) = \frac{\rho_g(\mathbf{x},t)}{\dfrac{1}{N(t)}\displaystyle\sum_{i=1}^{N(t)} g[\mathbf{x};\mathbf{x}_i(t)]}. \tag{A5}$$

In the simple case where the classification functional is set to unity, $\rho_g(\mathbf{x},t)$ reduces to the total density of trajectories. Another simple, but powerful approach, is to use the classification function to decompose the density. For example, a simple filter involves setting the classification function to one for trajectories that end up dissociating, and zero for those that scatter back. This gives a time-dependent density of reacting trajectories, as used in Fig. 6. Inverting the filter gives the density of backscattering trajectories.

In this study, we have barely scratched the surface of what is possible with this scheme by appropriate choices of classification functional. Filters, where the classification functional is either one or zero for all times, can be trivially formed to study any aspect of a reaction. For example, we have used filters to consider the time dependence of indirect and direct trajectories separately (results not presented). In a study of scattering states, it may be appropriate to filter out only trajectories that scatter back in a given dynamical state. For example, filtering out all those trajectories that end vibrationally excited should make it possible to determine which parts of a surface are most responsible for the vibrational excitation of molecules.

Other classification functionals can be based on dynamical quantities that vary with time along each trajectory. For example, we have previously visualized the time variation of kinetic energy,[23] where the classification functional is equal to the kinetic energy of the trajectory at time t. In such instances, it is more appropriate to use Eq. (A5), which gives a spatial expectation distribution of the dynamical quantity in question, in this case, kinetic energy. Other candidates for classification functionals of this type include vibrational-, rotational-, and translational energy.

It is also possible to use other time-dependent aspects of a trajectory that are not dynamical in nature, such as orientation. For example, a classification functional based on the

instantaneous polar angle of H$_2$ could be used to determine where and when molecules have a tendency to stand on end, rather than lie parallel to the surface.

[1] J. T. Yates, J. Vac. Sci. Technol. A **13**, 1359 (1995); C. R. Henry, Surf. Sci. Rep. **31**, 235 (1998); T. Zambelli, J. Wintterlin, J. Trost, and G. Ertl, Science **273**, 1688 (1996); B. E. Nieuwenhuys, Adv. Catal. **44**, 259 (2000); G. A. Somorjai, J. Phys. Chem. B **106**, 9201 (2002).

[2] S. L. Bernasek and G. A. Somorjai, J. Chem. Phys. **62**, 3149 (1975).

[3] I. E. Wachs and R. J. Madix, Surf. Sci. **58**, 590 (1976); K. Christmann and G. Ertl, Surf. Sci. **60**, 365 (1976).

[4] A. T. Gee and B. E. Hayden, J. Chem. Phys. **113**, 10333 (2000); A. T. Gee, B. E. Hayden, C. Mormiche, A. W. Kleyn, and B. Riedmuller, J. Chem. Phys. **118**, 3334 (2003).

[5] A. T. Gee, B. E. Hayden, C. Mormiche, and T. S. Nunney, J. Chem. Phys. **112**, 7660 (2000).

[6] A. T. Gee, B. E. Hayden, C. Mormiche, and T. S. Nunney, Surf. Sci. **512**, 165 (2002).

[7] G. J. Kroes, A. Gross, E. J. Baerends, M. Scheffler, and D. A. McCormack, Acc. Chem. Res. **35**, 193 (2002).

[8] P. Hohenberg and W. Kohn, Phys. Rev. **136**, B864 (1964); W. Kohn and L. J. Sham, Phys. Rev. **140**, A1133 (1965).

[9] P. H. T. Philipsen, G. Tevelde, and E. J. Baerends, Chem. Phys. Lett. **226**, 583 (1994); B. Hammer, M. Scheffler, K. W. Jacobsen, and J. K. Nørskov, Phys. Rev. Lett. **73**, 1400 (1994); J. A. White, D. M. Bird, M. C. Payne, and I. Stich, Phys. Rev. Lett. **73**, 1404 (1994); G. Wiesenekker, G. J. Kroes, E. J. Baerends, and R. C. Mowrey, J. Chem. Phys. **102**, 3873 (1995); S. Wilke and M. Scheffler, Surf. Sci. **329**, L605 (1995); A. Eichler, G. Kresse, and J. Hafner, Phys. Rev. Lett. **77**, 1119 (1996); W. Dong and J. Hafner, Phys. Rev. B **56**, 15396 (1997).

[10] A. Gross, S. Wilke, and M. Scheffler, Phys. Rev. Lett. **75**, 2718 (1995); A. Gross and M. Scheffler, Phys. Rev. Lett. **77**, 405 (1996); A. Gross, S. Wilke, and M. Scheffler, Surf. Sci. **358**, 614 (1996); A. Gross and M. Scheffler, Prog. Surf. Sci. **53**, 187 (1996); A. Gross, Surf. Sci. **363**, 1 (1996); A. Gross and M. Scheffler, Phys. Rev. B **57**, 2493 (1998); A. Gross, C. M. Wei, and M. Scheffler, Surf. Sci. **416**, L1095 (1998); A. Gross, Appl. Phys. A: Mater. Sci. Process. **67**, 627 (1998); M. Kay, G. R. Darling, S. Holloway, J. A. White, and D. M. Bird, Chem. Phys. Lett. **245**, 311 (1995); G. R. Darling, M. Kay, and S. Holloway, Surf. Sci. **400**, 314 (1998); M. Kay, G. R. Darling, and S. Holloway, J. Chem. Phys. **108**, 4614 (1998); C. Corriol, G. R. Darling, and S. Holloway, Surf. Sci. **532**, 198 (2003); L. Savio, L. Vattuone, L. Rocca, C. Corriol, G. R. Darling, and S. Holloway, Chem. Phys. Lett. **382**, 605 (2003); M. Beutl, M. Riedler, and K. D. Rendulic, Chem. Phys. Lett. **247**, 249 (1995); M. Beutl, J. Lesnik, E. Lundgren, C. Konvicka, P. Varga, and K. D. Rendulic, Surf. Sci. **447**, 245 (2000); M. Beutl, J. Lesnik, K. D. Rendulic, R. Hirschl, A. Eichler, G. Kresse, and J. Hafner, Chem. Phys. Lett. **342**, 473 (2001); R. Schennach, G. Krenn, B. Klotzer, and K. D. Rendulic, Surf. Sci. **540**, 237 (2003).

[11] A. Gross, J. Chem. Phys. **110**, 8696 (1999).

[12] H. F. Busnengo, W. Dong, and A. Salin, Chem. Phys. Lett. **320**, 328 (2000); C. Crespos, H. F. Busnengo, W. Dong, and A. Salin, J. Chem. Phys. **114**, 10954 (2001); H. F. Busnengo, E. Pijper, M. F. Somers, G. J. Kroes, A. Salin, R. A. Olsen, D. Lemoine, and W. Dong, Chem. Phys. Lett. **356**, 515 (2002); C. Diaz, F. Martin, H. F. Busnengo, and A. Salin, J. Chem. Phys. **120**, 321 (2004).

[13] H. F. Busnengo, C. Crespos, W. Dong, A. Salin, and J. C. Rayez, Phys. Rev. B **63**, 041402 (2001).

[14] H. F. Busnengo, W. Dong, P. Sautet, and A. Salin, Phys. Rev. Lett. **8712**, 127601 (2001).

[15] H. F. Busnengo, C. Crespos, W. Dong, J. C. Rayez, and A. Salin, J. Chem. Phys. **116**, 9005 (2002).

[16] C. Diaz, H. F. Busnengo, F. Martin, and A. Salin, J. Chem. Phys. **118**, 2886 (2003).

[17] M. A. Di Cesare, H. F. Busnengo, W. Dong, and A. Salin, J. Chem. Phys. **118**, 11226 (2003).

[18] H. F. Busnengo, E. Pijper, G. J. Kroes, and A. Salin, J. Chem. Phys. **119**, 12553 (2003).

[19] R. T. van Willigen, M. F. Somers, H. F. Busnengo, and G. J. Kroes, Chem. Phys. Lett. **393**, 166 (2004).

[20] H. F. Busnengo, A. Salin, and W. Dong, J. Chem. Phys. **112**, 7641 (2000).

[21] G. J. Kroes, E. J. Baerends, and R. C. Mowrey, J. Chem. Phys. **107**, 3309 (1997); G. J. Kroes, E. J. Baerends, and R. C. Mowrey, Phys. Rev. Lett. **78**, 3583 (1997); G. J. Kroes, M. R. Wall, J. W. Pang, and D. Neuhauser, J. Chem. Phys. **106**, 1800 (1997); D. A. McCormack, G. J. Kroes, and D. Neuhauser, J. Chem. Phys. **109** (13), 5177 (1998).

[22] D. A. McCormack, G. J. Kroes, E. J. Baerends, and R. C. Mowrey, Faraday Discuss. **110**, 267 (1998).

[23] R. A. Olsen, D. A. McCormack, and E. J. Baerends, Surf. Sci. **571**, L325 (2004).

[24] R. A. Olsen, H. F. Busnengo, A. Salin, M. F. Somers, G. J. Kroes, and E. J. Baerends, J. Chem. Phys. **116**, 3841 (2002).

[25] G. te Velde, Ph.D. Vrije Universiteit, 1990; G. T. Velde and E. J. Baerends, Phys. Rev. B **44**, 7888 (1991); G. te Velde, and E. J. Baerends, J. Comput. Phys. **99**, 84 (1992).

[26] A. D. Becke, Phys. Rev. A **38**, 3098 (1988).

[27] J. P. Perdew, Phys. Rev. B **33**, 8822 (1986); J. P. Perdew, Phys. Rev. B **33**, 8822(E) (1986).

[28] R. A. Olsen, S. C. Badescu, S. C. Ying, and E. J. Baerends, J. Chem. Phys. **120**, 11852 (2004).

[29] R. A. Olsen, G. J. Kroes, and E. J. Baerends, J. Chem. Phys. **111**, 11155 (1999).

[30] G. Kresse, Phys. Rev. B **62**, 8295 (2000); P. Riviere, H. F. Busnengo, and F. Martin, J. Chem. Phys. **121**, 751 (2004); M. Luppi, R. A. Olsen, and E. J. Baerends, Phys. Rev. B (submitted).

[31] A. Press, S. Teukolsky, W. Vetterling, and B. Flannery, *Numerical Recipes in Fortran 77*, 2nd ed. (Cambridge University Press, New York, 1992).

[32] D. A. McCormack and G. J. Kroes, Chem. Phys. Lett. **296**, 515 (1998).

[33] J. M. Bowman, B. Gazdy, and Q. Y. Sun, J. Chem. Phys. **91**, 2859 (1989); W. H. Miller, W. L. Hase, and C. L. Darling, J. Chem. Phys. **91**, 2863 (1989); T. D. Sewell, D. L. Thompson, J. D. Gezelter, and W. H. Miller, Chem. Phys. Lett. **193**, 512 (1992); R. Alimi, A. Garciavela, and R. B. Gerber, J. Chem. Phys. **96**, 2034 (1992); A. J. C. Varandas, J. Chem. Phys. **99**, 1076 (1993); A. J. C. Varandas and J. M. C. Marques, J. Chem. Phys. **100**, 1908 (1994); D. L. Shen, W. T. Chan, and H. O. Pritchard, J. Chem. Soc., Faraday Trans. **91**, 3747 (1995); Y. Guo, D. L. Thompson, and T. D. Sewell, J. Chem. Phys. **104**, 576 (1996); K. F. Lim and D. A. McCormack, J. Chem. Phys. **102**, 1705 (1995); D. A. McCormack and K. F. Lim, J. Chem. Phys. **103**, 1991 (1995); D. A. McCormack and K. F. Lim, J. Chem. Phys. **106**, 572 (1997); D. A. McCormack and K. F. Lim, Phys. Chem. Chem. Phys. **1**, 1 (1999); C. Schlier, J. Chem. Phys. **103**, 1989 (1995); M. Bennun and R. D. Levine, J. Chem. Phys. **101**, 8768 (1994); M. BenNun and R. D. Levine, J. Chem. Phys. **105**, 8136 (1996); G. Stock and U. Muller, J. Chem. Phys. **111**, 65 (1999); U. Muller and G. Stock, J. Chem. Phys. **111**, 77 (1999).

[34] A. Gross and M. Scheffler, J. Vac. Sci. Technol. A **15**, 1624 (1997).

[35] G. R. Darling and S. Holloway, Surf. Sci. **304**, L461 (1994).

[36] K. Svensson, L. Bengtsson, J. Bellman, M. Hassel, M. Persson, and S. Andersson, Phys. Rev. Lett. **83**, 124 (1999); L. Bengtsson, K. Svensson, M. Hassel, J. Bellman, M. Persson, and S. Andersson, Phys. Rev. B **61**, 16921 (2000).

[37] A. C. Luntz, J. K. Brown, and M. D. Williams, J. Chem. Phys. **93**, 5240 (1990).

[38] P. Samson, A. Nesbitt, B. E. Koel, and A. Hodgson, J. Chem. Phys. **109**, 3255 (1998).

[39] E. Pijper, G. J. Kroes, R. A. Olsen, and E. J. Baerends, J. Chem. Phys. **117**, 5885 (2002); S. M. Kingma, M. F. Somers, E. Pijper, G. J. Kroes, R. A. Olsen, and E. J. Baerends, J. Chem. Phys. **118**, 4190 (2003).

[40] W. Schroeder, K. Martin, and B. Lorensen, *The Visualization Toolkit: An Object-Oriented Approach to 3D Graphics*, 3rd ed. (Pearson Education, Inc., 2002).

[41] Kitware, Visualization Toolkit (VTK) (http://www.kitware.com/vtk/).

[42] IBM, OPENDX (http://www.opendx.org).